Simulation for LArTPC experiments

Final Report for the Summer Student Internship 2016

Student: Lucas Mendes Santos
Supervisor: Carlos Escobar

October 4, 2016

Contents

Chapter 1

Introduction

Neutrinos are one of the particles of interest for at least 70 years. From its first proposal by Pauli (which, by the way, assumed it was a desperate explanation for the energy deficit saw in beta decay experiments) to being one of the particles that hints that the universe is more than what we thought. As years pass by, more and more tweaks on the neutrino physics leads us to physics beyond a standard model of particle physics[8].

1.1 Neutrino Physics

Neutrinos are leptons with no electric charge which interacts through only the weak and gravitational channels. From the standard model point of view they are particles which forms doublets with each one of the known leptons, i.e. $e, \mu, \tau \rightarrow \nu_e, \nu_\mu, \nu_\tau$, with no mass. However due to its property of oscillation it is known that they do have a small but considerable mass. Thus, if we consider that the neutrinos can be represented by two orthonormal basis:

- Flavor Eigenstates $(\nu_e, \nu_\mu, \nu_\tau)$
- Mass Eigenstates (ν_1, ν_2, ν_3)

There is a non-zero probability that a neutrino produced in a ν_α flavor eigenstate can be detected as a ν_β eigenstate on a defined energy E and distance L from the source

$$P(\nu_\alpha \rightarrow \nu_\beta) = \left| \sum_i U^*_{\beta j} e^{\frac{i m_j^2 L}{2E}} U_{\alpha j} \right|^2 \tag{1.1}$$

The $U_{\alpha j}$ are elements of the PMNS (Pontecorvo–Maki–Nakagawa–Sakata) matrix[13, 15]

$$U = \begin{pmatrix} 1 & 0 & 0 \\ 0 & c_{23} & s_{23} \\ 0 & -s_{23} & c_{23} \end{pmatrix} \begin{pmatrix} c_{13} & 0 & s_{13} e^{-i\delta_C P} \\ 0 & 1 & 0 \\ -s_{13} e^{-i\delta_C P} & 0 & c_{13} \end{pmatrix} \begin{pmatrix} c_{12} & s_{12} & 0 \\ -s_{12} & c_{12} & 0 \\ 0 & 0 & 1 \end{pmatrix} \tag{1.2}$$

where $s_{ij} = sin\ \theta_{ij}$, $c_{ij} = cos\ \theta_{ij}$ and δ_{CP} is the CP violation phase.

Since the formulation and proof of this phenomenon, major collaborations, like Sudbury Neutrino Observatory (SNO)[12], Super-Kamiokande[10], KamLAND[2], Double Chooz[7], Reno[3], Daya Bay[4], T2K[1] and MINOS[14] made an effort to accurately measure these parameters by analysis of various sources of neutrinos. Recently, the collaboration Daya Bay[5] through electronic antineutrinos oscillation analysis brought up with high precision the value of the last unknown mixing angle (θ_{13}).

1.2 Neutrino Physics Today

Even though the recent experiments bring up all the parameters in 1.2 through the possibility of measuring the probability of oscillation (or survival) of a neutrino 1.1, still there is some loose ends.

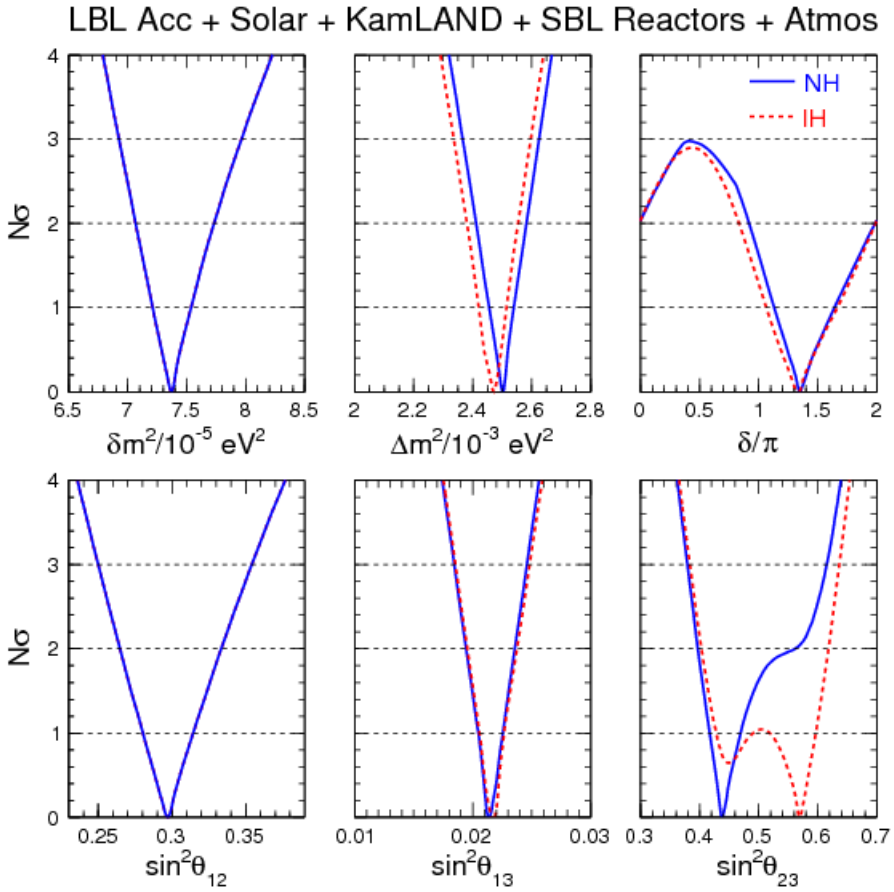

Figure 1.1: Global fitting of the oscillation parameters (δm^2 stands for Δm^2_{12} and $\Delta m^2 = m^2_3 - \frac{m^2_1+m^2_2}{2}$). Figure extracted from reference [9].

As seen in figure 1.1, some parameters needs more precision. For example, in a 3σ confidential level[1], neutrinos can ($\delta_{CP} \neq 0,\ \pi$) or cannot ($\delta_{CP} = 0,\ \pi$) violate CP. This parameter has a extremely importance because if neutrinos have this property, i would be a candidate to explain the matter-antimatter asymmetry on the universe.

Furthermore, it's not known the mass ordering of the neutrinos in the mass representation. Some parameters, for example θ_{23} are strongly dependent if neutrinos have a normal ($m_1 < m_2 < m_3$) or inverted ($m_3 < m_1 < m_2$) mass hierarchy.

Thus, the need of more precise experiments is of utmost importance.

[1]Probability of roughly 99% of a certain value being in a particular interval.

Chapter 2

Liquid Argon Time Projection Chambers

Proposed by Rubbia in 1977[17], Liquid Argon Projection Chambers (LArTPC) represent a ideal alternative for detection when it comes to neutrino physics. These detectors when deployed in underground laboratories can be used both for studies of neutrino astrophysicists as proton decay. Liquid argon detectors have great ability to identify particles, calorimetric resolution and scalability to very large sensitive volumes. However, technology must be fully developed and understood so that it can be used in all its capacity.

2.1 Why use Liquid Argon Time Projection Chambers?

Liquefied argon is very attractive particle detector media as it uniquely combine a number of properties and due to be relatively cheap. As a noble element, it provides a high stopping power for ionizing radiation, described by their high density ρ, short radiation X_0 and nuclear interaction $\lambda_i nt$ lengths. This results in a large energy loss per unit distance dE/dx for traversing ionizing particles and, taking into account the value W_e, describing the amount of energy needed to produce an electron-ion pair, in a relatively large number of quasifree electrons (See Table 2.1 for more details).

Atomic Number	18
Molecular Weight	39.948 g/mol
Natural Concentration	0.934% of air volume
Liquid Density (at 83.7 K)	1392.8 kg/m^3
dE/dx for m.i.p[1]	2.12 MeV/c^2
Light Yield	40000 γ's/MeV
Ionization energy W_e $(E = \infty)$	23.6 eV
Excitation energy W_γ (E = 0)	19.5 eV
Radiation length X_0	14 cm
Nuclear interaction length $\lambda_i nt$	84 cm

Table 2.1: Physical properties of argon

Apart from the high ionization yield, argon offers an excellent scintillation yield and it is transparent to the light it produces[2] . Being a noble element, it does not tend to attach electrons due to a fully occupied valence shell which gives a high electron mobility, it allows an efficient transport of electrons across long distances which is an aspect of major relevance for TPCs. Moreover, the technology to strongly reduce the level of impurities in noble liquids is readily available.

[2]The photons produced don't have the energy to excite the electrons

2.2 How does it work?

A TPC consists of two parallel planes (cathode and anode) separated by a drift gap (Figure 2.1). While the anode is connected to ground, the cathode is biased to a high negative electric potential to set up an electric field within the detector active volume. The field strength is typically of the order of several 100 V/cm for the largest drift gaps and up to a few 10 kV/cm for the smallest ones.

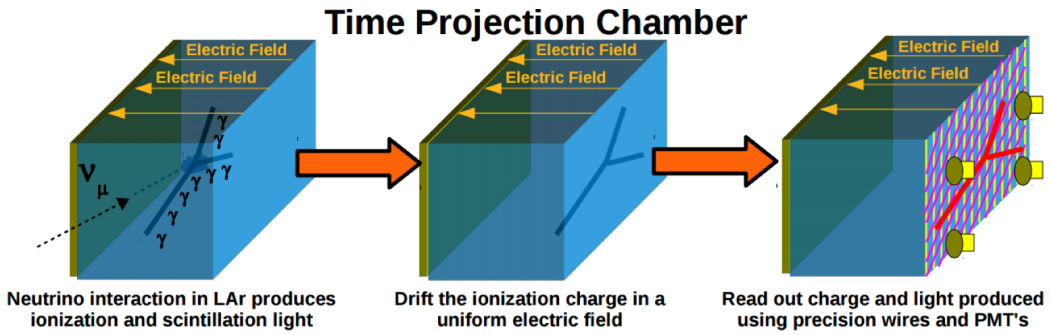

Figure 2.1: Schematic of functionality of a LArTPC.

An ionizing particle traversing a LArTPC creates pairs of positively charged argon ions Ar^+ and quasifree electrons e^- along its path (ionization track). In a analogous situations, an argon atom may be raised to an excited state instead of being ionized, which eventually leads to the emission of argon scintillation light during its de-excitation. Moreover, scintillation light can be produced by the recombination of an electric field dependent amount of electron-ion pairs.

As said before, liquid argon is transparent to the light it produces ($\lambda = 128$ nm), thus the scintillation light can be measured by photodetectors to use it as a trigger, to provide the precise event time stamp t_0 and to gain additional information about an event to facilitate its reconstruction.

The residual electrons and argon cations, left after recombination, are separated by the presence of the electric field forcing them to drift towards the anode or the cathode respectively, each one with a particular drift velocity[3]. Comparing their velocities, electrons have a much higher mobility than the ions which for an overall detector performance is favorable, making the electrons the particle of choice for reading out bringing the ionization track information. Furthermore, it is necessary a high uniformity of the electric field for the integrity of the original ionization track. Any field non uniformity would cause distortions of the track and strongly affect the detector spatial resolution.

During the drift, two physics processes have an impact on the detector performance. Firstly, the drifting electrons are subject to longitudinal (along the drift direction) and transverse (perpendicular to the drift direction) diffusion. This limits the spatial resolution of the device. Secondly, electronegative impurities, such as oxygen and water molecules dissolved in the sensitive liquid argon volume, tend to attach electrons and thus reduce the amount of charge drifting to read out. Consequently, impurities diminish the detector output signals and hence one is interested in keeping their concentration in the device as low as possible.

2.2.1 Reading out the events

The scintillation process, in a simplified model, can happen by direct excitation by the ionizing radiation and recombination of the electron-ion pairs (see Figure 2.2).

In both cases, the intermediate state is given by an argon atom in its first excited state Ar^*. In triple collisions with surrounding argon atoms, the excited argon atom can change its electronic configuration and form an excimer Ar_2^* in a ps timescale (Equation 2.1).

$$Ar^* + 2Ar \rightarrow Ar_2^* + Ar \tag{2.1}$$

This excimer is a bound state and can be on singlet ($^1\Sigma_u^+$) or on a triplet $^3\Sigma_u^+$ with different lifetimes before de-excitation process[11].

[3]It's an average considering all the phenomena that can happen during their trajectory as acceleration phases, interrupted collisions so on and so forth.

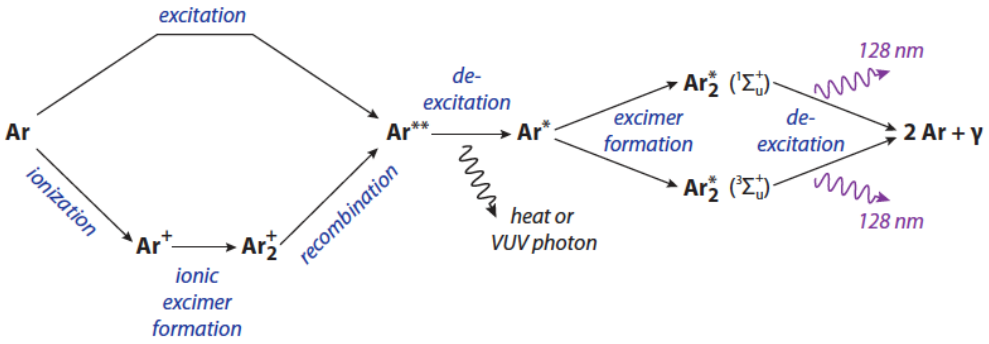

Figure 2.2: Simplified picture of the main scintillation mechanisms in liquefied argon.

$$Ar_2^*(^1\Sigma_u^+) \rightarrow Ar_2(^1\Sigma_g^+) + \gamma \rightarrow 2Ar + \gamma \tag{2.2}$$

$$Ar_2^*(^3\Sigma_u^+) \rightarrow Ar_2(^1\Sigma_g^+) + \gamma \rightarrow 2Ar + \gamma \tag{2.3}$$

The singlet transition to the ground state $Ar_2(^1\Sigma_g^+)$ (Equation 2.2) of the dimer is fast ($\sim ns$) while the triplet transition to $Ar_2(^3\Sigma_g^+)$ (Equation 2.3) is suppressed and therefore slow ($\sim \mu s$), therefore scintillation light on liquid argon has a fast and slow component. The light produced due to the scintillation process is on the VUV[4] region with a peak around 128 nm wuth a width of 7 nm to 10 nm, hence as the usual photodetectors are not optimized for this wavelength, the use of wavelength shifters is mandatory. Photondetectors usually found on LArTPC experiments are photomultiplier tubes (PMT), Silicon Photomultipliers and acrylic bars.

On the other hand, for reading out the drifted electrons, a collection of wireplanes are used. A wireplane is an array (grid) of thin conductive parallel wires separated by typically 2 mm to 4 mm from each other. To realize segmentation along different spatial coordinates, the read-out configuration consists of two (induction + collection) or three wireplanes (2 induction + collection) of different orientations separated by a small gap of up to a few mm.

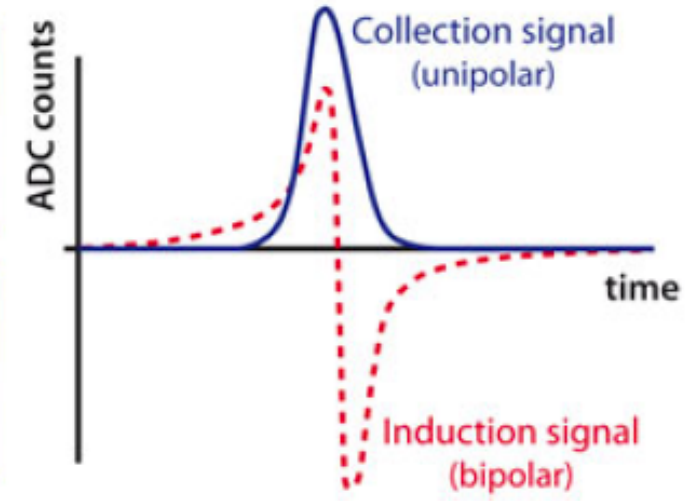

Figure 2.3: Examples of bipolar induction (red dashed line) and unipolar collection (blue solid line) modes.

An electron generated in the detector volume follows the applied uniform drift field and approaches induction plane which is set to ground potential. To make sure that the electrons are not collected already, the collection must be biased to a positive potential to produce an electric field

[4]Vacuum Ultra Violet

between the two planes. The moving charge carriers approaching the induction plane induce currents in the wires located at the corresponding spatial coordinates. Once the electrons have passed through the wireplane, the electric current in the wires is reversed, thus giving a bipolar signal. As long as the transparency condition is met, none of the drifting charge carriers are collected here and the read-out is said to be non-destructive or operated in induction mode (hence the name). At the third wireplane the electrons are finally collected (collection mode, destructive readout) which is why the induced signals from the wires of the collection are unipolar. To resolve ambiguities in the event reconstruction, a setup with three wire grids U, V, X (two in induction and one in collection mode) is usually chosen. The two induction planes U and V, mostly anti-symmetric, are at specific angles with respect to the collection plane.

For a wireplane configuration typically set up for LArTPCs, a track induced by a minimum ionizing particle leads to a number of about 6000 electrons per wire at the read-out[16] which gives a charge of 1 fC approximately. Thus, for reading out the wireplanes signals is necessary a front-end electronic to amplify the signal.

2.3 Neutrino Precision Era and the LArTPCs

In its modus operandi, a LArTPC detector have the possibility of a full 3D-imaging (wireplanes plane projection + electron drift timing), excellent particle identification (PID) which is based entirely on the topology of the event and capability and precise calorimetric energy reconstruction represents the most advanced experimental technology for neutrino physics.

2.3.1 Electromagnetic shower and photons separation

LArTPCs have the ability to distinguish between electromagnetic from photon induced showers. It is a key point to short baseline and long baseline neutrino experiments (Figure 2.4). The first phenomena corresponds to the expected signal from charged-current interactions of electron neutrinos while the latter corresponds to the principal background from neutral pions produced in neutral-current interactions of all neutrino flavors.

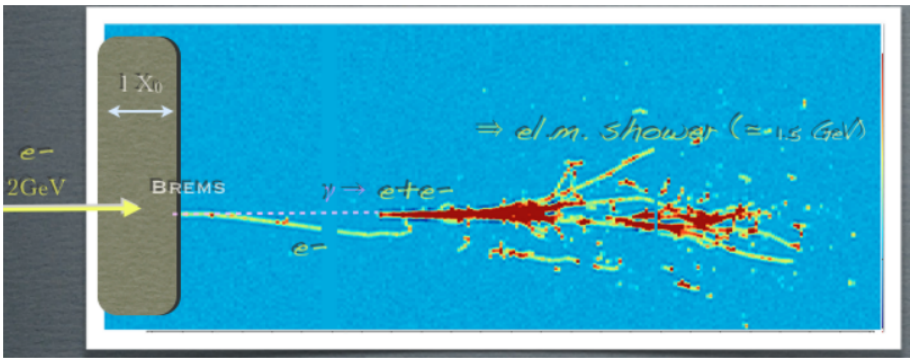

Figure 2.4: MC simaluation of a photon-shower induced by electron bremsstrahlung in the LArTPC. The parent electron enters from the left. The photon conversion into a electron-positron pair initiates a shower that is well separated in the LArTPC volume from the parent electron track and shower.

One good thing in using this technology is that only initial part of the shower is relevant for separating these categories because the photon converts to an electron-positron pair producing double ionization in the first portion of the track where the two particles overlap at the shower start.

2.3.2 Charge sign determination

The sign of a particle's charge can be obtained for stopping particles in LArTPC by statistical analysis based on topological criteria, even without a magnetic field (Figure 2.5). For example, μ^+ undergo decay only, with e^+ emission of known energy spectrum. Stopping μ^- may either decay or be captured by nuclei. In Ar, the capture probability is about 76%, accompanied by neutron

and γ emission. The μ^--capture can thus be topologically separated from μ^+-decay through the detection of a delayed Michel electron track in the LArTPC.

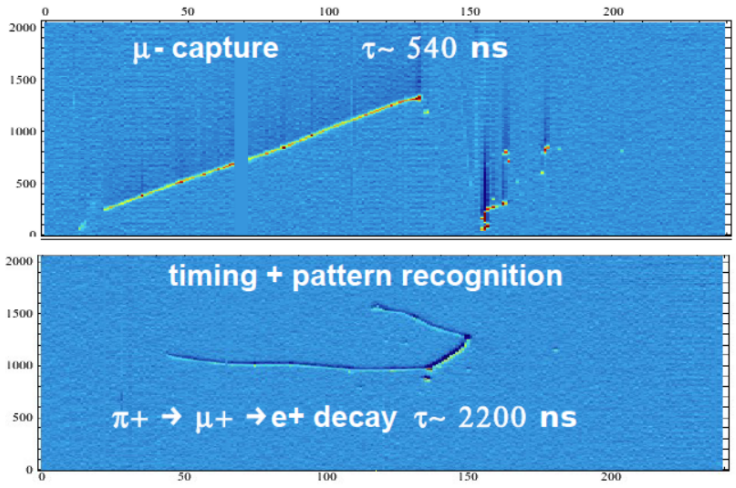

Figure 2.5: Extracted from ArgoNeuT[6] data: Capture-like events topology (Upper), decay-like event topology (Bottom).

2.3.3 Particle Identification

When charged hadrons propagate through liquid argon and come to stop without inelastic interaction within the LArTPC volume, the energy deposited along the fully contained track can be combined with the range information from three dimensional tracking to compare the kinetic energy to the total range of the track as well as to compare the dE/dx to the residual range of the track (Figure 2.6).

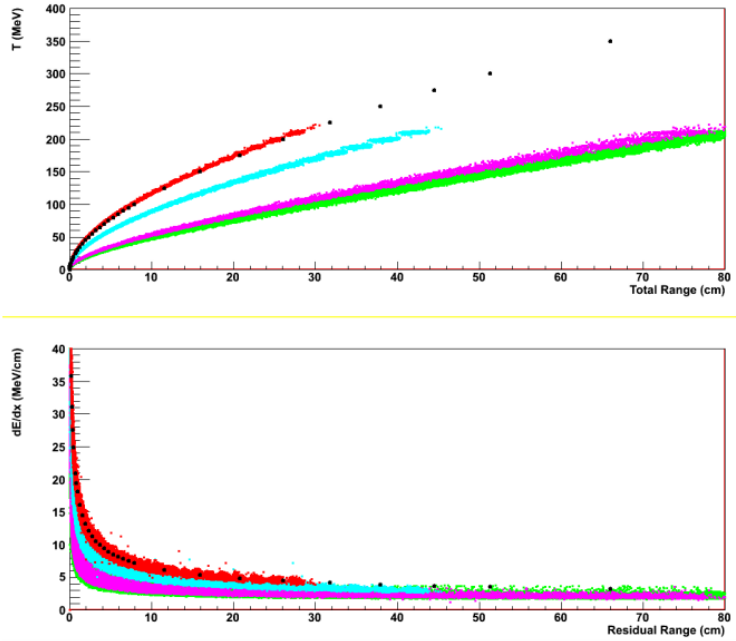

Figure 2.6: The deposited kinetic energy as a function of the total track range (top) and the dE/dx as a function of the residual track range (bottom) for μ(green), π(violet), K(cyan) and p(red).

Efficient particle identification can be obtained using these measurements and this technique represents one of the key features of the LArTPC technology that is relevant for both neutrino oscillation experiments and proton decay searches.

Chapter 3

Acquiring know how - The Liquid Argon In A Testbeam Experiment (LArIAT)

As seen in the last chapter, a LArTPC is a strongly candidate for a precise neutrino detection. However, the technology must be completely developed and characterized. So, as part of an integrated plan of developing these detectors, accurate measurements in LArTPC of known particle species, in the relevant energy ranges for neutrino detection, is necessary.

3.1 The LArIAT

The Liquid Argon In A Testbeam (LArIAT) experiment was created to achieve these goals by deploying a LArTPC detector in a dedicated calibration test beam line at Fermilab. All the measurements done on the experiment are significant for the neutrino oscillation program in the US, from the Short Baseline Neutrino (SBN) program (MicroBooNE, SBND and ICARUS) to Long Baseline Experiments as DUNE in the long term.

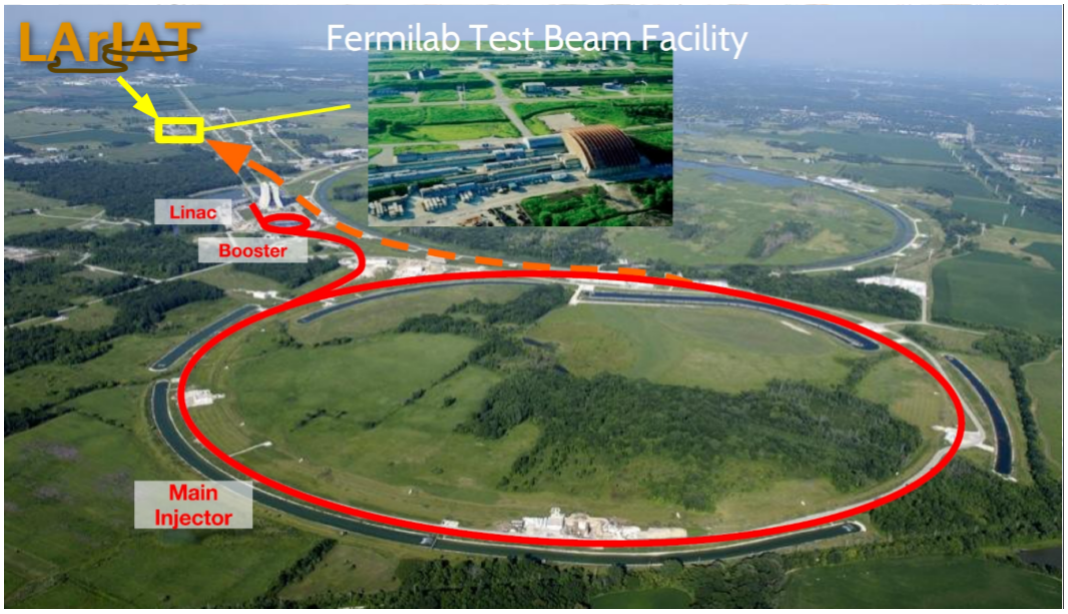

Figure 3.1: The Fermilab Facility Testbeam

The main objectives of LArIAT can be summarized as:

- R&D Goals
  - Improvement of the energy resolution through the combination of scintillation light and ionization charge signals
  - Optimization of particle ID techniques
  - Study of LArTPC event reconstruction and calorimetry systematics
- Physics Goals
  - Measurement of charged hadron-Ar interaction cross sections and study of exclusive channels: first $\pi^{\pm}$-Ar total cross section measurement, studies on π absorption;
  - π^0 production via $\pi^{\pm}$ charge exchange;
  - Kaon identification and interaction topology study for baryon number violation searches (e.g. proton decay);
  - e/γ shower identification for neutrino oscillation experiments
  - μ sign determination in the absence of a magnetic field, using topology (decay vs capture)
  - Study of nuclear effects and Final State Interaction in Ar that will provide cross section constraints and systematic uncertainties estimates for particles produced in neutrino interactions
  - Geant4 validation for hadrons interaction models and simulation

3.1.1 The Secondary and Tertiary Beams

The LAriAT Experiment is located in the Fermilab Test Beam Facility (Figure 3.1). The test beam is composed basically by protons with 120 GeV/c momentum. Entering the facility it hits a primary copper target where the secondary beam, consisted mostly of pions from 8 to 32 GeV, is produced (Figure 3.2).

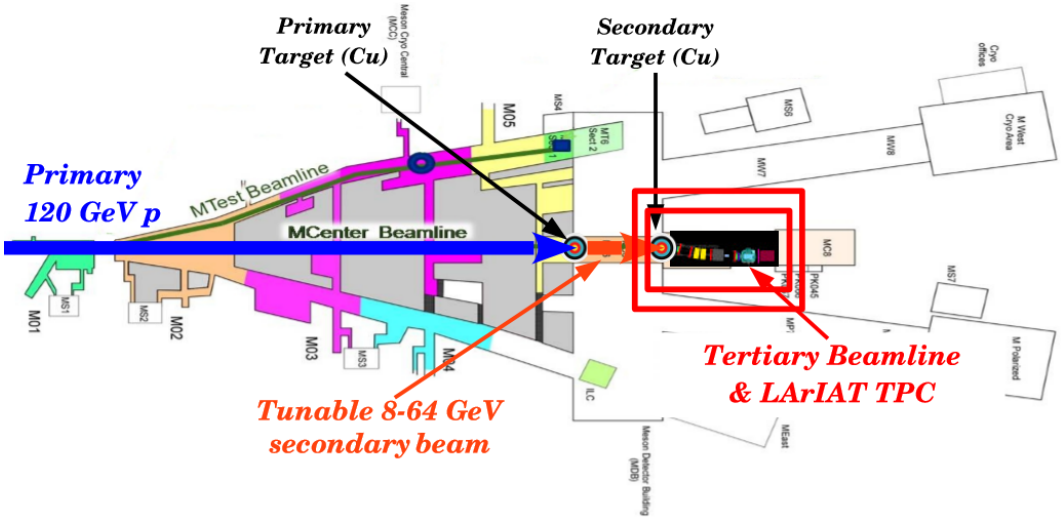

Figure 3.2: The secondary beam. Fromt he secondary beam one has the power to choose the energy range of particles hitting the secondary target. This is very useful for studying the by products of neutrino interactions in different ranges of energy and distance from the source.

This secondary beam can be tunable, so one can tune it up to energies relevant to experiments of Short baseline as well long Baseline neutrino oscillation experiments (Figure 3.3(a)). This secondary beam them will hit a secondary copper target which will bring forth the tertiary beam comprised of mostly pions $\pi^{\pm}$ along with a mix of muons $\mu^{\pm}$, protons (p), kaons $K^{\pm}$, and electrons $e^{\pm}$ in the range 200 MeV to 2 GeV. The tertiary beam is where LArIAT is located (Figure 3.3(b)).

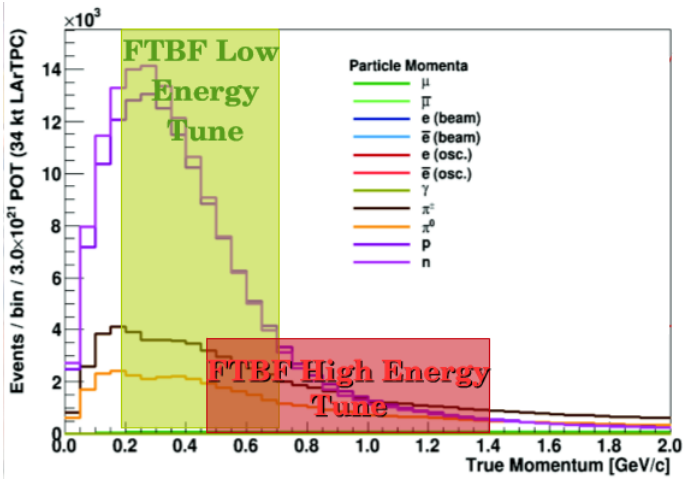

(a) Momenta Spectra of particles from the secondary beam. This beam is tunable to energy ranges that is relevant for neutrino physics experiments.

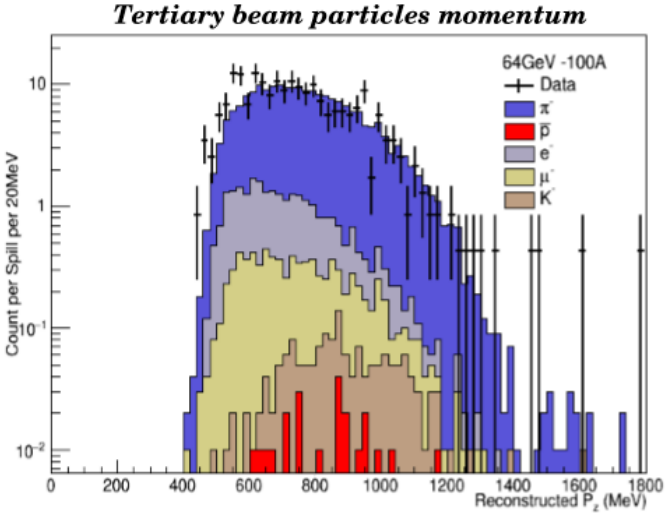

(b) Momenta spectra of the particles from the tertiary beam. This is the energy range of detection for LArIAT.

Figure 3.3: Particle momenta information present on the Fermilab Test Beam Facility.

3.1.2 The LArTPC and Beamline Detectors

The LArIAT TPC is hosted in a vacuum-insulated cryostat, filled with LAr. It has an active volume of 47 cm x 40 cm x 90 cm. There are two anode wire planes (Induction and Collection) which are instrumented with dedicated cold electronics to collect the drifting electrons inside the TPC. Each of the two planes consist of 240 wires oriented at $\pm 60°$ relative to the beam axis, with 4 mm anode wire spacing.

The LArIAT light collection system consists of an array of two high quantum efficiency cryogenic photomultiplier tubes (PMT) and three Silicon PhotoMultiplier Detectors (SiPM), which are deployed in Liquid Argon and mounted behind the wire planes of the TPC (Figure 3.4(b)).

The beamline detectors (Figure 3.5) are comprised of different detectors which one with a specific purpose. The ones that are currently being used for data analysis and event selection are the Time of Flight detectors (TOF) and the Multi Wire Proportional Chambers (MWPC) or Wire Chambers for short (WC), The main purpose of these detectors is to characterize the particle prior entering the TPC, so one can correlate the information given by these detectors to the physics phenomena that happened inside the TPC. The other detectors main purpose is to further discriminate between pions and muons.

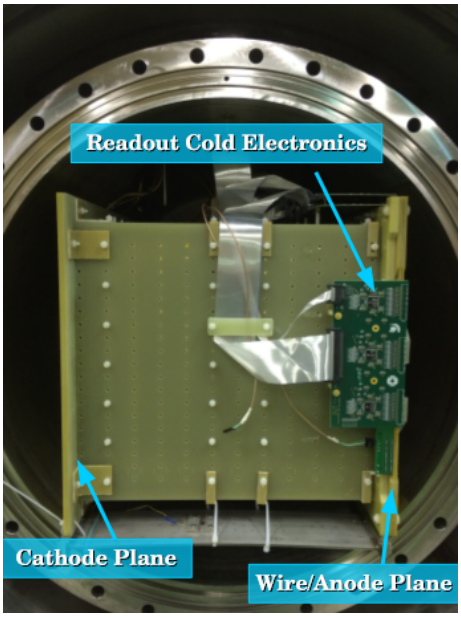

(a) The LArIAT TPC. The TPC is a refurbished version of ArgoNeuT

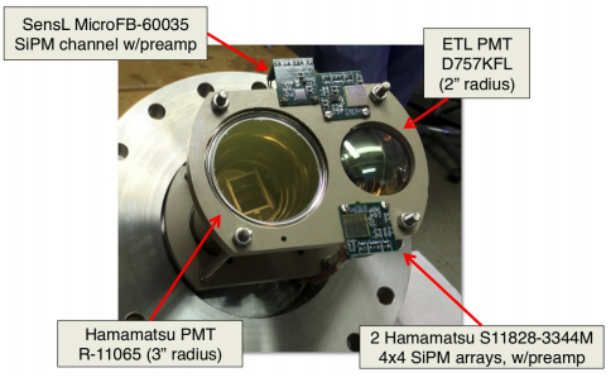

(b) Momenta spectra of the particles from the tertiary beam. This is the energy range of detection for LArIAT.

Figure 3.4: The LArIAT Cryostat.

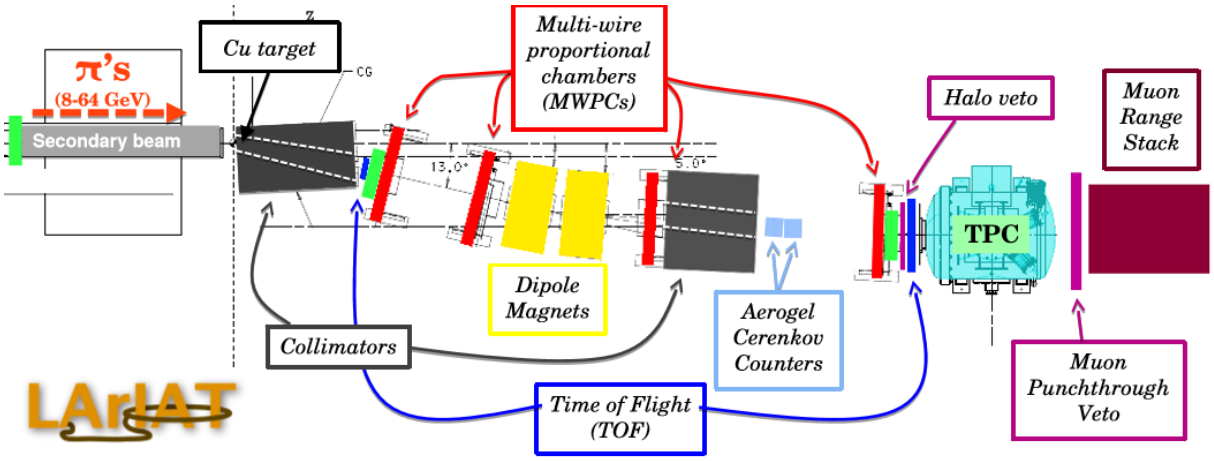

Figure 3.5: The LArIAT Schematics. The TPC is surrounded by a variety of detectors. Their main purpose is to identify and characterize the particles that interacts inside the TPC. This way, there can be a correlation between a particle information entering the detector and all the physics that happens inside of it.

The Multi Wire Proportional Chambers

A MWPC is a detector consisted of two planes (cathode and anode) separated by a thin gap which is filled with a gaseous element. The anode is made by wires in a similar fasshion as the TPC. As a charged particle passes through each wire chamber, it induces a signal on a nearby wire in each chamber. This signal can give a x-y position of the passage of the particle through the detector. The combination of the subsequent particle position in each wire chambers before (2) and after (2) the magnets gives us the trajectories of the particle before and after the bending. Combining this with the magnetic field imposed by the dipole magnets is possible to calculate the momentum of the particle. Using the magnets is possible to change its polarity, so there can be a charge selection of the particles reaching the TPC.

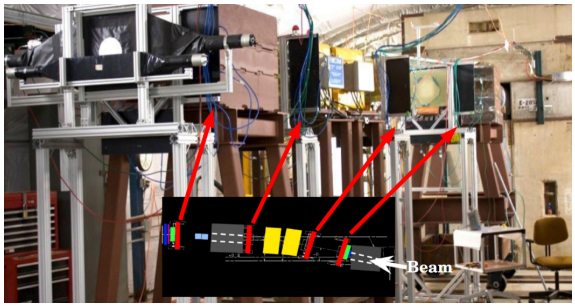

Figure 3.6: The Wire Chamber Detectors. The main purpose of this detectors is when used in conjunction with the dipole magnets, can give the particle momentum information.

The Time Of Flight Detectors

The Time of Flight detector is comprised of two scintillating plastic paddles (the Upstream and Downstream detectors) coupled with photomultiplier tubes (Four PMTs for upstream and two for downstream) (Figure 3.7). Time of Flight (TOF) provides a clock for how long a particle takes to travel through the beamline (Figure 3.8(a)).

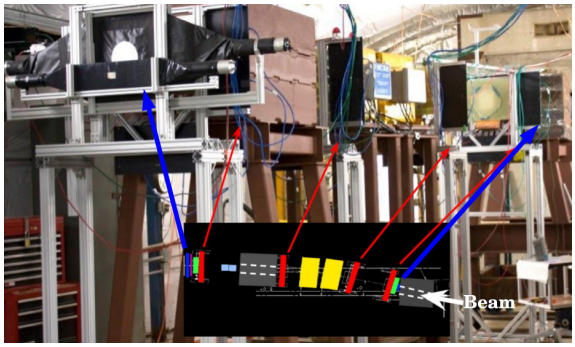

Figure 3.7: The Time of Flight Detectors. They serve as a clock for the timing of particle reaching the TPC.

When used in conjunction with the WC, both detectors can do particle identification prior entering the TPC (Figure 3.8(b)).

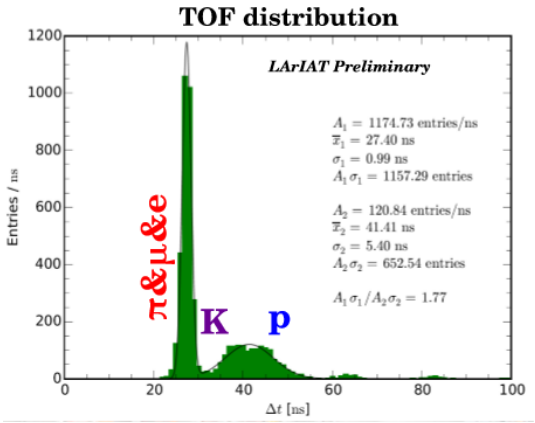

(a) Time of Flight of different particles.

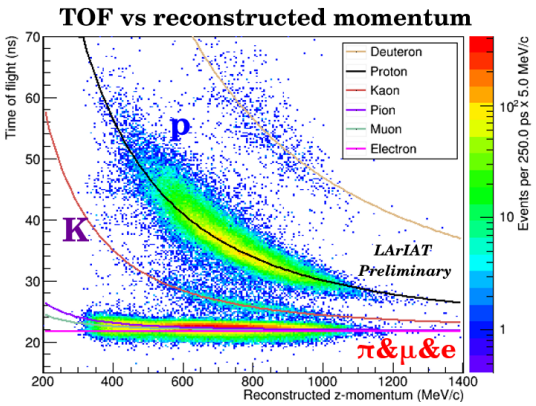

(b) Momenta spectra of the particles from the tertiary beam. This is the energy range of detection for LArIAT.

Figure 3.8: The LArIAT Cryostat.

3.2 The Beamline Simulation

Until now, all the simulations doing on LArIAT was shooting particles in the TPC directly. However, the collaboration thrived for a full experiment simulation, taking into account all the detectors in the beamline, not only the TPC. For that, it was necessary to simulate the electronics of each one of the detectors. The main purpose was to validate all the reconstruction methods for the beamline detectors besides a more accurate correlation between simulation and data.

The Time of Flight Simulation

The simulation of the electronics of TOF detectors used waveform profiles took from data. Took the waveforms information using a fitting function over data (3.1).

$$ADC(time) = Baseline - Constant \times Landau(time, peak\ time, sigma) \tag{3.1}$$

The profiles then were implemented on the simulation so each occurrence of a simulated particle passing through the TOF detectors it would produce a signal represented by one of the sampled waveforms.

To validate the simulation, it was compared the reconstruction of the time of flight using the same algorithm used in data and compared that to the truth value of the simulation (Figure 3.9).

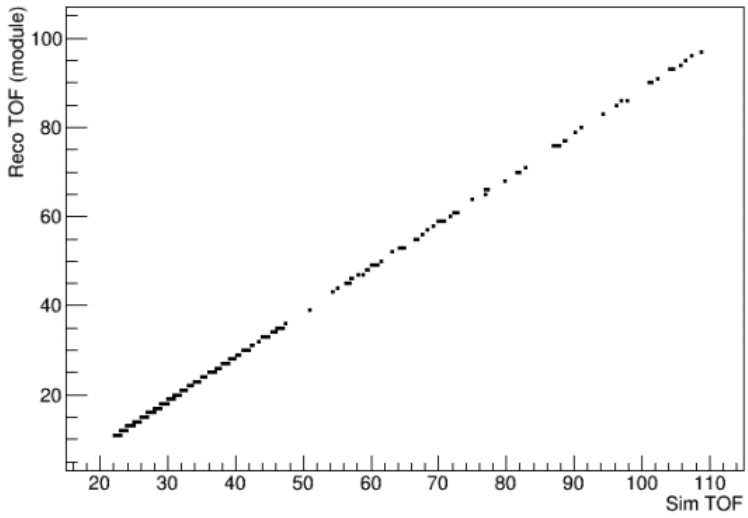

Figure 3.9: Comparison between the reconstructed time of flight and the truth time from the simulation. There is a deficit of 10 ns between them. This is put ad hoc on the reconstruction algorithm due to different drift times of the photoelectrons inside the PMTs.

As one can see there is a good agreement between the parameters except for a difference of 10 ns order. This value is known by the collaboration, which comes forth from the algorithm reconstruction. The explanation of putting this *ad hoc* is to take into account the intrinsic characteristics of the different photomultipliers used into the two detectors where wach model has a different transit time of the photoelectrons form the photocathode to the first dynode.

3.2.1 The Time of Flight Offset

Referring to this feature of TOF, a study was suggested to determine more precisely the apparent displacement of the reconstruction with the actual time of flight of the particle.

For this, data was taken from cosmic rays using the two detectors in a telescope configuration. As the detectors were very close to each other is expected that any time difference between them is due to this offset (Figure 3.10).

Clearly there are at least two regions of interest shown by the settings, why this happens is still on research. One solution would be a new take data for greater statistical terms. This will be done in the coming months.

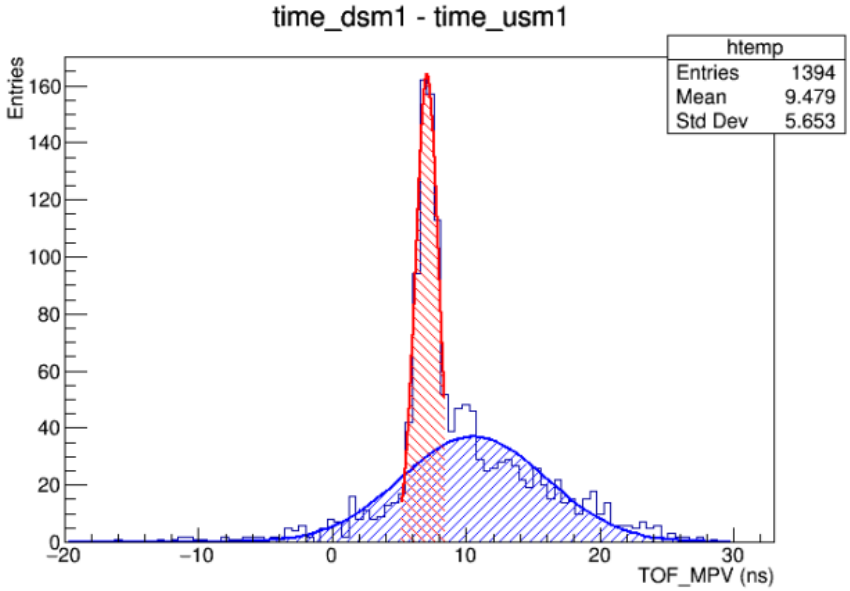

Figure 3.10: Time difference between the detectors. The timing for each one of the detectors is represented by the TOF_MPV which represents the peak time of the waveform.

Regarding the simulation itself, the next steps will be to verify a correlation between the setting parameters to the number of photons produced by the passage of different particles. If such a correlation exists there is a possibility to make a much more realistic simulation.

3.3 The 2 Magnets approach momentum reconstruction

The currently momentum reconstruction method, take into account the 4 MWPCs. However, instead of considering the individual bends that each one magnet does to the particle trajectory, it is considered as the particle passed through only one magnet in a effective length. The work done here was to propose a new method considering the presence of the two magnets individually.

The method itself defines a plane with their normal parallel to the beam direction which is located between the two electromagnets. Using the input and output angles of the particles entering and leaving the electromagnets combined with the magnetic fields of the two magnets, it is estimated an intermediate angle particle to pass through the fictional plane (3.2).

$$\theta_c = \frac{(1-\epsilon)\theta_e + (1+\epsilon)\theta_l}{2} \tag{3.2}$$

Where ϵ defines the difference (in field intensity) between the magnets, θ_e is the entering angle and $theta_l$ is the leaving angle. Following that, it is estimated the momentum of the particle passing separately in each of the magnets (3.3).

$$p = \frac{\int Bdl}{sin\ \theta_e - sin\ \ \theta_l} \tag{3.3}$$

Finally, the final momentum is calculated taking the simple average of the two momenta.

For validation, it was checked how profound was the effect using this new approach when compared with the previous one. It was found that when the magnets would have a 0.5% difference in between their field intensity and also selecting events that the particle left a signal in all MWPC's (Picky Tracks), it was verified that the difference between the methods is about 1% (Figure 3.11).

Also a scatter plot was made to find any correlation between the methods (Figure 3.12). The methods are quite linear between itself, except for a shift of the order of 2 MeV/c. The possibility of this characteristic to persist even changing ϵ to other values and situations where one of the MWPC's produced no signal is under investigation at the moment.

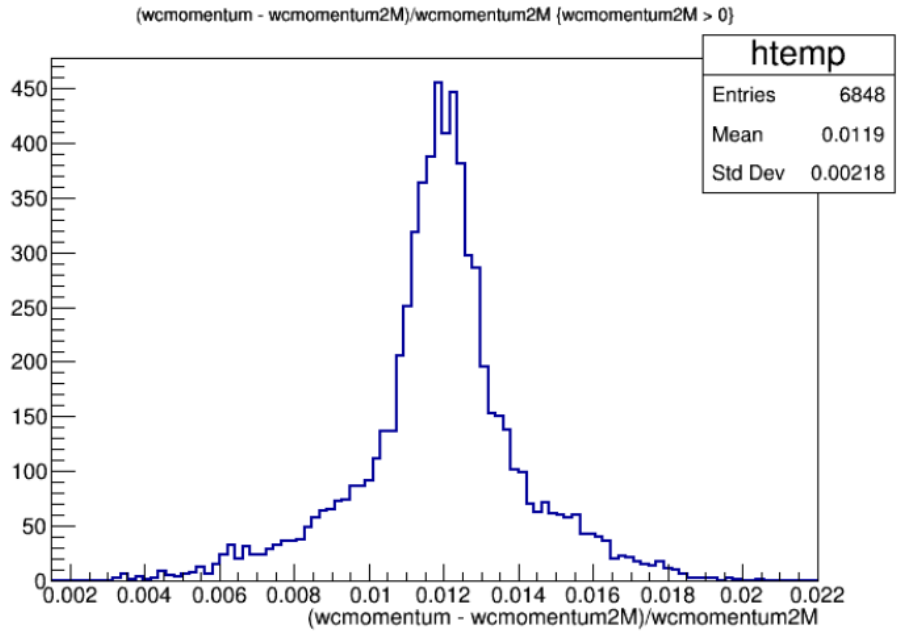

Figure 3.11: The normalized difference between methods. WCmomentum stands for the Wire Chamber momentum reconstruction using the one magnet approximation. WCMomentum2M is for the 2 magnets approximation.

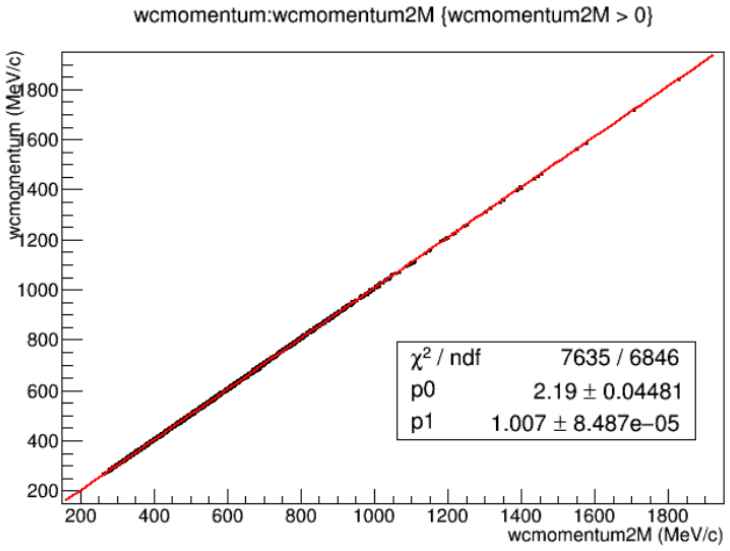

Figure 3.12: Scatter plot between the two methods. The methods appear to bem very linear to each other besides a shift of 2 MeV/c.

Chapter 4

Conclusions

The neutrino physics is an area of constant expansion. The need of better experiments with better precision is fundamental to complete this theory. Achieving the goal will give a better perspective of how the universe works and its origin.

The LArTPC detector is a very useful tool and candidate to fulfill this requirements with its great 3D-imaging reconstruction, partical identification power and calorimetry. However, it still needs fully development characterization to be scalable to higher masses as will e used on the DUNE experiment. Walking through this path, the LArIAT experiment comes to give more knowledge on the functionality of this technology though the detection of charged particles that is candidates to appear in the neutrino interaction with the active volume.

All the simulation development done to this experiment, is personal useful for gaining software experience. With the framework experience one can be more able to lead new analysis not just for this experiment as well for other experiments inserted on the neutrino program. Furthermore, all the development is useful for the experiment as weel, as other collaborators can use this advancements for their own research.

Bibliography

[1] K. Abe et al. The T2K Experiment. *Nucl. Instrum. Meth.*, A659:106–135, 2011.

[2] S. Abe et al. Precision Measurement of Neutrino Oscillation Parameters with KamLAND. *Phys. Rev. Lett.*, 100:221803, 2008.

[3] J. K. Ahn et al. Observation of Reactor Electron Antineutrinos Disappearance in the RENO Experiment. *Physical Review Letters*, 108(19):191802, May 2012.

[4] F. P. An, Q. An, J. Z. Bai, A. B. Balantekin, H. R. Band, W. Beriguete, M. Bishai, S. Blyth, R. L. Brown, G. F. Cao, and et al. A side-by-side comparison of Daya Bay antineutrino detectors. *Nuclear Instruments and Methods in Physics Research A*, 685:78–97, Sept. 2012.

[5] F. P. An et al. Observation of electron-antineutrino disappearance at Daya Bay. *Phys. Rev. Lett.*, 108:171803, 2012.

[6] C. Anderson et al. The ArgoNeuT Detector in the NuMI Low-Energy beam line at Fermilab. *JINST*, 7:P10019, 2012.

[7] F. Ardellier et al. Double Chooz: A Search for the neutrino mixing angle theta(13). 2006.

[8] L. M. Brown. The idea of the neutrino. *Physics Today*, 31:23–28, Sept. 1978.

[9] F. Capozzi, E. Lisi, A. Marrone, D. Montanino, and A. Palazzo. Neutrino masses and mixings: Status of known and unknown 3ν parameters. *Nucl. Phys.*, B908:218–234, 2016.

[10] S. Fukuda et al. The Super-Kamiokande detector. *Nuclear Instruments and Methods in Physics Research A*, 501:418–462, Apr. 2003.

[11] A. Hitachi. Exciton kinetics in condensed rare gases. *The Journal of Chemical Physics*, 80(2), 1984.

[12] N. Jelley, A. B. McDonald, and R. H. Robertson. The sudbury neutrino observatory. *Annual Review of Nuclear and Particle Science*, 59(1):431–465, 2009.

[13] Z. Maki, M. Nakagawa, and S. Sakata. Remarks on the Unified Model of Elementary Particles. *Progress of Theoretical Physics*, 28:870–880, Nov. 1962.

[14] D. G. Michael et al. Observation of muon neutrino disappearance with the MINOS detectors and the NuMI neutrino beam. *Phys. Rev. Lett.*, 97:191801, 2006.

[15] B. Pontecorvo. Inverse beta processes and nonconservation of lepton charge. *Sov. Phys. JETP*, 7:172–173, 1958. [Zh. Eksp. Teor. Fiz.34,247(1957)].

[16] V. Radeka, H. Chen, G. Deptuch, G. D. Geronimo, F. Lanni, S. Li, N. Nambiar, S. Rescia, C. Thorn, R. Yarema, and B. Yu. Cold electronics for "giant" liquid argon time projection chambers. *Journal of Physics: Conference Series*, 308(1):012021, 2011.

[17] C. Rubbia. The Liquid Argon Time Projection Chamber: A New Concept for Neutrino Detectors. 1977.